REPORT DOCUMENTATION PAGE

Form Approved
OMB No. 0704-0188

1. REPORT DATE *(DD-MM-YYYY)*	**2. REPORT TYPE**	**3. DATES COVERED** *(From - To)*
June 2012	Technical Paper	June 2012-August 2012

4. TITLE AND SUBTITLE
Design and Verification Methodology of Boundary Conditions for Finite Volume Schemes

5a. CONTRACT NUMBER
In-House

5b. GRANT NUMBER

5c. PROGRAM ELEMENT NUMBER

6. AUTHOR(S)
Folkner, D., Katz, A and Sankaran, V.

5d. PROJECT NUMBER

5e. TASK NUMBER

5f. WORK UNIT NUMBER
3002125K

7. PERFORMING ORGANIZATION NAME(S) AND ADDRESS(ES)

Air Force Research Laboratory (AFMC)
AFRL/RQR
5 Pollux Dr.
Edwards AFB CA 93524-7048

8. PERFORMING ORGANIZATION REPORT NO.

9. SPONSORING / MONITORING AGENCY NAME(S) AND ADDRESS(ES)
Air Force Research Laboratory (AFMC)
AFRL/RQR
5 Pollux Drive
Edwards AFB CA 93524-7048

10. SPONSOR/MONITOR'S ACRONYM(S)

11. SPONSOR/MONITOR'S REPORT NUMBER(S)
AFRL-RZ-ED-TP-2012-236

12. DISTRIBUTION / AVAILABILITY STATEMENT
Distribution A: Approved for Public Release; Distribution Unlimited. PA#12720

13. SUPPLEMENTARY NOTES
Conference paper for the Seventh International Conference on Computational Fluid Dynamics (ICCFD7), Hawaii, USA, 9-13 July 2012.

14. ABSTRACT
Despite the critical importance of resolving flow at or near domain boundaries, often boundary condition formulations are implemented in an ad-hoc fashion. The purpose of this work is to provide a general framework for the implementation and, importantly, the verification of boundary conditions for node- and cell-centered finite volume schemes. These conditions may include any combination of Dirichlet conditions, Neumann conditions, extrapolation, and in some instances, the conservation equations themselves. Specific conditions for inviscid walls, inflow, and outflow are systematically tested using manufactured and exact solutions. The procedures in this work provide a method for the verification of complex boundary conditions as well as shed valuable physical insight for different problem situations.

15. SUBJECT TERMS

16. SECURITY CLASSIFICATION OF:			**17. LIMITATION OF ABSTRACT**	**18. NUMBER OF PAGES**	**19a. NAME OF RESPONSIBLE PERSON**
					Shawn Phillips
a. REPORT	**b. ABSTRACT**	**c. THIS PAGE**			**19b. TELEPHONE NO** *(include area code)*
Unclassified	**Unclassified**	**Unclassified**	SAR	21	661-275-5621

Standard Form 298 (Rev. 8-98)
Prescribed by ANSI Std. 239.18

Seventh International Conference on Computational Fluid Dynamics (ICCFD7), Big Island, Hawaii, July 9-13, 2012

ICCFD7-2012-1001

Design and Verification Methodology of Boundary Conditions for Finite Volume Schemes

D. Folkner*, A. Katz* and V. Sankaran**
Corresponding author: david.folkner@aggiemail.usu.edu

* Utah State University, USA.
** Air Force Research Laboratory, USA.

Abstract: Despite the critical importance of resolving flow at or near domain boundaries, often boundary condition formulations are implemented in an ad-hoc fashion. The purpose of this work is to provide a general framework for the implementation and, importantly, the verification of boundary conditions for node- and cell-centered finite volume schemes. These conditions may include any combination of Dirichlet conditions, Neumann conditions, extrapolation, and in some instances, the conservation equations themselves. Specific conditions for inviscid walls, inflow, and outflow are systematically tested using manufactured and exact solutions. The procedures in this work provide a method for the verification of complex boundary conditions as well as shed valuable physical insight for different problem situations.

Keywords: Boundary Conditions, Finite Volume, Lagrange Multipliers, Manufactured Solutions, Verification.

1 Introduction

Computational fluid dynamics (CFD) is used to simulate flows for a variety of applications. Often, these applications require high levels of accuracy at or near domain boundaries. Examples of such applications include calculations of aerodynamic lift and drag, computation of boundary layer profiles, estimation of heating at surface locations, and mass flux computation. For these and other cases, the region near the boundary is the primary focus of the CFD simulation. Although the computational domain may extend greatly from these boundaries, the areas near them often require the greatest resolution and numerical accuracy.

Despite the need for high accuracy near boundaries (or perhaps because of it), numerous boundary procedures have been proposed in the literature. For example, a widely used inviscid wall treatment by Rizzi [1] involves the use of the momentum equation to obtain the pressure. Jameson directly modified the flux at an inviscid wall to involve no convective contribution [2]. Alternately, Dadone and Grossman advocate a curvature corrected symmetry condition for an inviscid wall [3]. Balakrishnan and Fernandez advocate a variety of other methods for an inviscid wall involving additional quantities such as entropy and enthalpy [4]. Numerous other strategies exist for inviscid walls as well as other boundary conditions, such as inflow, outflow, and no-slip walls. The difficulty is that many of these methods have not been rigorously verified and may or may not be consistent with the interior discretization schemes. Recently, Choudhary et. al. [5] successfully verified boundary conditions using the method of manufactured solutions (MMS). Their approach requires carefully constructed manufactured solutions that already satisfy the boundary conditions, which means that a new manufactured solution needs to be constructed for each boundary condition and geometry.

This work addresses many of these difficulties by focusing on three main goals. First, we provide a general framework for implementation of boundary conditions for both node- and cell-centered schemes. The framework applies to arbitrary boundary conditions for any physical system. Second, we provide a rigorous

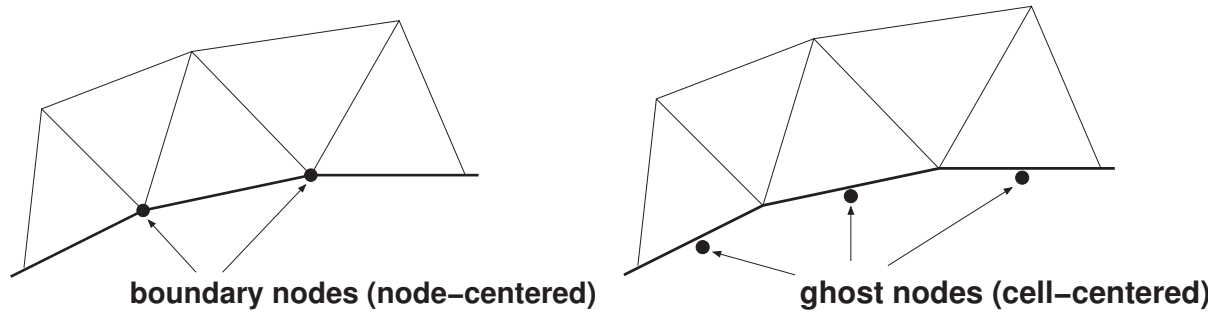

(a) Boundary degrees of freedom for node-centered methods. (b) Boundary ghost nodes for cell-centered methods.

Figure 1: Location of boundary condition enforcement for node- and cell-centered schemes.

and general approach for the verification of these boundary conditions based on MMS. While verification is an essential step in CFD development and practice, many verification strategies have neglected boundary effects [6, 7, 8, 9, 10]. In this work we extend the traditional use of MMS to include boundary conditions and uncover certain key aspects of using MMS in this way. While the verification procedure determines the numerical accuracy of the discretization, it does not indicate that the proper equations have been selected for a given problem. Therefore, the third objective of this work is to demonstrate the requirement of choosing physically correct boundary conditions for a given problem. Unlike the interior, at boundaries, the choice of governing equations is not well established. The studies in this work indicate that the choice of boundary conditions is not unique, but careful analysis is necessary to verify the properties of these formulations.

In order to accomplish these tasks, we explore the formulation of a variety of common boundary types, including inviscid walls, inflow, and outflow, for both node- and cell-centered finite volume schemes. For each of these boundary types, we explore a variety of conditions spanning Dirichlet, Neumann, and extrapolation. Importantly, we highlight the fact that node-centered schemes allow for direct use of the governing equations of motion (mass, momentum, and energy) themselves at the boundaries. Cell-centered schemes do not easily allow use of the equations of motion, but usually rely on extrapolation or other conditions. Great care must be taken with cell-centered schemes to avoid the selection of additional conditions, which may conflict with the interior equations of motion. Other boundary condition types and implementations beyond those discussed in this work are certainly possible. Here, the principal objective is to provide a framework for the implementation and verification of any boundary condition.

The paper is organized as follows: First, boundary condition formulations are explored for node- and cell-centered finite volume schemes. We present a common discretization framework with which we test a variety of governing boundary equations. We show how to verify these boundary conditions using MMS. We then present a number of grid refinement studies. First a quasi-1D nozzle is tested with both MMS and exact solutions. Next, we extend the use of MMS to two dimensions and wall boundary conditions. Finally we present error convergence results using Ringleb flow and a NACA 0012 subsonic airfoil. We then offer some conclusions derived from these studies.

2 Boundary Condition Implementation

In this work we test a variety of boundary condition implementations and assess the resulting impact on accuracy through rigorous verification studies. In the interior of the domain, we solve the steady Euler equations,

$$\frac{\partial Q}{\partial \tau} + \boldsymbol{\nabla} \cdot \boldsymbol{F} = 0, \tag{1}$$

where $Q = (\rho, \rho u, \rho v, \rho e)^T$ is the vector of conserved variables, and $\boldsymbol{F}$ is the inviscid flux vector. Here, ρ is density, u and v are the Cartesian velocity components, and e is the total energy per unit mass. We are interested in solving the steady equations to which we add the pseudo-time (τ) derivative for convenience in marching to steady state. We test both node- and cell-centered finite volume spatial discretizations, which

result in a semi-discrete set of non-linear equations of the form

$$\frac{\partial Q}{\partial \tau} + R(Q) = 0, \tag{2}$$

where $R(Q)$ is the steady residual at either an interior node or an interior cell location depending on the discretization procedure.

In addition to the interior discretization scheme, we must also incorporate boundary conditions to close the system of equations on a finite domain. Here we focus on inviscid wall, inflow, and outflow conditions in order to explore fundamental issues of physical and numerical accuracy. The methodology developed here is quite general and directly applies to other boundary condition types as well. For node-centered discretizations, boundary conditions are enforced directly at the boundary nodes coincident with the physical boundary, shown in Figure 1(a). For cell-centered discretizations, we introduce additional unknowns in the form of ghost nodes located at the flux quadrature points of the boundary faces, shown in Figure 1(b). The ghost nodes are then used in an upwind flux formula to determine the numerical flux through the boundary face. In this manner, the cell-centered boundary formulation remains water-tight. The node-centered configuration, however, is not strictly water-tight since the fluxes surrounding the boundary nodes do not always cancel with nearby interior nodes.

For both node- and cell-centered formulations, we define a "boundary residual," $R_b(Q)$, which we drive to zero at steady state along with the interior residuals, $R(Q)$:

$$R_b(Q) = 0. \tag{3}$$

At boundaries in a node-centered discretization, R_b replaces R at the boundary nodes. In cell-centered discretizations, R_b provides the governing equations for the ghost nodes. In all, we test fifteen different boundary implementations, which are listed with a common notational convention in Table 1 for clarity. The methods all involve Dirichlet-specified quantities, with the state specification completed by other methods, such as Neumann conditions, extrapolation, or combinations of the equations of motion. We will refer to this table as we develop various forms for R_b in the following sections.

Table 1: Notation for boundary condition methods tested.

Short Name	Boundary Type		Dirichlet	Other conditions
n-INV1	Node-centered	Inviscid wall	u_n	Lagrange multipliers
n-INV2	Node-centered	Inviscid wall	u_n	u_t Neumann, mass and energy eqs.
n-INV3	Node-centered	Inviscid wall	u_n	$\rho, u_t, \rho e$ Neumann
n-INV4	Node-centered	Inviscid wall	–	zero convective flux
n-INF1	Node-centered	Inflow	s, h, u_t	Lagrange multipliers
n-INF2	Node-centered	Inflow	s, h, u_t	outgoing characteristic eq.
n-OUT1	Node-centered	Outflow	p	Lagrange multipliers
n-OUT2	Node-centered	Outflow	p	outgoing characteristic eqs.
c-INV1	Cell-centered	Inviscid wall	u_n	$\rho, u_t, \rho e$ extrapolated
c-INV2	Cell-centered	Inviscid wall	–	Pressure extrapolated
c-INV3	Cell-centered	Inviscid wall	u_n	$\rho, u_t, \rho e$ Neumann
c-INF1	Cell-centered	Inflow	s, h, u_t	u_n extrapolated
c-INF2	Cell-centered	Inflow	R^-, u_t, s	R^+ extrapolated
c-OUT1	Cell-centered	Outflow	p	ρ, u, v extrapolated
c-OUT2	Cell-centered	Outflow	R^-	R^+, u_t, s extrapolated

2.1 Node-Centered Boundaries

All boundary conditions involve the specification of a certain number of Dirichlet (or Neumann) conditions augmented by additional information derived from the interior field. With node-centered schemes it is straightforward to select a combination of the governing equations of motion (mass, momentum, and energy)

to enforce at boundary nodes. This is because the boundary nodes lie within control volumes for which we can easily implement flux balances. This will be shown in the methods described below. In contrast, cell-centered boundary conditions often require the use of ghost nodes for which there is no natural control volume or flux balance. Thus, it becomes difficult to apply the equations of motion directly at the ghost nodes. Instead, we choose some other method to define the ghost node state, such as extrapolation.

Enforcement of boundary conditions within a node-centered scheme involves the specification of the boundary residual, R_b, directly at the boundary nodes shown in Figure 1(a). In this section, we outline two procedures to obtain the boundary residual. The first involves the use of Lagrange multipliers as discussed in detail by Allmaras [11]. The second involves the multiplication of the governing equations of mass, momentum, and energy by a selection matrix to complete the boundary conditions. In addition, we discuss a third method involving a commonly used weak boundary condition for an inviscid wall.

2.1.1 Lagrange Multipliers

A method of boundary condition enforcement that has enjoyed widespread use in the finite element community for several decades is the Lagrange multiplier method introduced by Babuska [12]. The extension of this method to the Navier-Stokes equations was discussed in detail by Allmaras [11], but seems to have received little attention in the finite volume community. The reader is reffered to the above sources for details. It suffices to state here that the method involves a modification of the variational statement to include extra conditions along Dirichlet boundaries, leading to an extended system of the form

$$\left\{ \begin{array}{c} B(Q) - b \\ \frac{\partial Q}{\partial \tau} + R(Q) + \left(\frac{\partial B}{\partial \tilde{Q}} \right)^T \lambda \end{array} \right\} = 0. \tag{4}$$

Here, $B(Q) - b$ represents a vector of m additional Dirichlet conditions that must be satisfied at boundary nodes. For example, at a fixed inviscid wall, $m = 1$, $B(Q) = \boldsymbol{u} \cdot \boldsymbol{n}$, and $b = 0$. The additional m conditions are incorporated via a vector of m Lagrange multipliers, λ. The choice of variables for $\tilde{Q}$ in Equation 4 produces different conditions. While Allmaras chooses entropy variables, $\tilde{Q} = \frac{\rho}{p}(\frac{p}{\rho}\frac{\gamma+1-s}{\gamma-1} - e, u, v, -1)^T$, other variables, such as the primitive variables, $\tilde{Q} = (P, u, v, T)^T$, are possible, leading to different boundary equations. Thus, the Lagrange multiplier method does not appear to uniquely define the boundary equations.

While the extended system in Equation 4 can be solved directly to include the Lagrange multipliers, these may be eliminated from the problem altogether, resulting in a boundary residual form,

$$R_b(Q) = \left\{ \begin{array}{c} B(Q) - b \\ N \left(\frac{\partial Q}{\partial \tau} + R(Q) \right) \end{array} \right\}. \tag{5}$$

Here, N is a $(n - m) \times n$ matrix containing a basis for the nullspace of the boundary condition matrix, such that

$$N \left(\frac{\partial B}{\partial \tilde{Q}} \right)^T = 0. \tag{6}$$

In essence, the Lagrange multiplier method provides a way to augment Dirichlet boundary conditions with some combination of the equations governing mass, momentum and energy. The Lagrange multiplier method is easily applied to the node-centered formulation because it makes use of the discretized equations of motion, $R(Q)$, at the boundary nodes. As previously stated, N depends upon the choice of $\tilde{Q}$, resulting in different boundary residuals.

A novel aspect of this work is the verification of boundary conditions through rigorous grid refinement studies. We do this for exact solutions which are available for certain simple configurations. However, we desire a more general method that is applicable to a wide variety of boundary conditions and flow equations that do not possess exact solutions. To accomplish this, we extend our previous work using the method of manufactured solutions (MMS) [13], to include boundary conditions. This enables the use of a single arbitrary manufactured solution to simultaneously verify the accuracy of both the interior scheme and boundary conditions. This is accomplished by adding an MMS source term to both the Euler and boundary

equations:

$$\frac{\partial Q}{\partial \tau} + \boldsymbol{\nabla} \cdot \boldsymbol{F} = S(\boldsymbol{x})$$
$$B(Q) - b = S_b(\boldsymbol{x}) \tag{7}$$

For the Lagrange multiplier method this results in a modified boundary residual of the form

$$R_b(Q) = \begin{Bmatrix} B(Q) - b - S_b(\boldsymbol{x}) \\ N\left(\frac{\partial Q}{\partial \tau} + R(Q) - S(\boldsymbol{x})\right) \end{Bmatrix}. \tag{8}$$

The proposed method of boundary verification does not require that the manufactured solution satisfy the boundary conditions as required by other approaches[5]. This greatly simplifies the verification procedure, and allows a single manufactured solution to be used to verify any number of boundary conditions.

We test three boundary conditions that make use of the Lagrange multiplier methodology. These are denoted n-INV1, nINF1, and n-OUT1. Method n-INV1 for a node-centered inviscid wall sets the normal velocity to zero and retains a combination of the mass, momentum, and energy equations:

$$B(Q) = u_n, \quad b = 0, \quad N = \begin{pmatrix} 1 & 0 & 0 & 0 \\ 0 & n_y & -n_x & 0 \\ 0 & -u & -v & 1 \end{pmatrix}. \tag{9}$$

Here, $\boldsymbol{n} = (n_x, n_y)^T$ is the outward pointing unit normal vector at the surface node, and $u_n = n_x u + n_y v$ is the velocity in the normal direction.

The subsonic inflow condition n-INF1 specifies entropy, s, total enthalpy, h, and tangential velocity, $u_t = -n_y u + n_x v$:

$$B(Q) = \begin{pmatrix} h \\ s \\ u_t \end{pmatrix}, \quad b = \begin{pmatrix} h_{spec} \\ s_{spec} \\ u_{t,spec} \end{pmatrix}, \quad N = \begin{pmatrix} u_n h & u_t v - n_x(h + \frac{1}{2}q^2) & -u_t u - n_y(h + \frac{1}{2}q^2) & u_n \end{pmatrix} \tag{10}$$

Here, the subscript *spec* denotes a specified value and q is the velocity magnitude.

The final method using Lagrange multipliers is n-OUT1 for subsonic outflow. This method fixes static pressure,

$$B(Q) = p, \quad b = p_{spec}, \quad N = \begin{pmatrix} -u & 1 & 0 & 0 \\ -v & 0 & 1 & 0 \\ -h & 0 & 0 & 1 \end{pmatrix}. \tag{11}$$

Again, we emphasize that the method of Lagrange multipliers provides an automatic way to determine a complete set of boundary equations. Once we determine $B(Q)$ and a set of variables $\tilde{Q}$, the remaining equations are fixed through the nullspace, N. However, the actual form of N is dependent on the choice of $\tilde{Q}$, which appears to be arbitrary. Further work is needed to determine which set of $\tilde{Q}$ and the resulting N is best suited for various conditions.

2.1.2 Selection Matrix Method

A more intuitive method to obtaining a boundary residual is through a selection matrix that picks desired combinations of the equations of motion. Using a selection matrix, A, we define the boundary residual as

$$R_b(Q) = \Omega(Q) + A\left(\frac{\partial Q}{\partial \tau} + R(Q)\right). \tag{12}$$

Here, A selects certain combinations of the equations of motion which augment other boundary conditions, $\Omega(Q)$. These conditions may be Dirichlet (D), Neumann (N), or extrapolated (E):

$$\Omega(Q) = \Omega_D(Q) + \Omega_N(Q) + \Omega_E(Q). \tag{13}$$

Whereas the Lagrange multiplier approach only accommodates Dirichlet conditions, this framework allows for general specification of virtually any type of boundary condition imaginable. It should be noted that the Lagrange multiplier method is a subset of this more general approach, where $\Omega_D(Q) = B(Q) - b$, and $A = N$ augmented with rows of zeros.

This more general form is also easily modified for verification via MMS by introducing source terms for $\Omega(Q)$ and the equations of motion themselves:

$$R_b(Q) = \Omega(Q) - S_b(\boldsymbol{x}) + A\left(\frac{\partial Q}{\partial \tau} + R(Q) - S(\boldsymbol{x})\right). \tag{14}$$

Here, $S_b(\boldsymbol{x})$ acts on the $\Omega(Q)$ terms, and $S(\boldsymbol{x})$ acts on the governing equations of motion.

We test four node-centered boundary conditions that make use of the selection matrix method. These are denoted n-INV2, n-INV3, n-INF2 and n-OUT2. For n-INV2, a Neumann condition is set only for the tangential velocity terms, while the mass and energy equations are used directly:

$$\Omega_D(Q) = \begin{pmatrix} 0 \\ 0 \\ u_n \\ 0 \end{pmatrix}, \quad \Omega_N(Q) = \begin{pmatrix} 0 \\ \partial u_t/\partial n \\ 0 \\ 0 \end{pmatrix}, \quad \Omega_E(Q) = 0, \quad A = \begin{pmatrix} 1 & 0 & 0 & 0 \\ 0 & 0 & 0 & 0 \\ 0 & 0 & 0 & 0 \\ 0 & 0 & 0 & 1 \end{pmatrix} \tag{15}$$

In this manner, velocity is treated with a symmetry condition while mass and energy are conserved. These types of symmetry conditions enforced with Neumann conditions have been advocated by many other researchers for slip walls in inviscid flows [14, 15, 16].

Method n-INV3 uses Neumann conditions for all equations, completely omitting any contribution from the Euler equations:

$$\Omega_D(Q) = \begin{pmatrix} 0 \\ 0 \\ u_n \\ 0 \end{pmatrix}, \quad \Omega_N(Q) = \begin{pmatrix} \partial \rho/\partial n \\ \partial u_t/\partial n \\ 0 \\ \partial(\rho e)/\partial n \end{pmatrix}, \quad \Omega_E(Q) = 0, \quad A = \begin{pmatrix} 0 & 0 & 0 & 0 \\ 0 & 0 & 0 & 0 \\ 0 & 0 & 0 & 0 \\ 0 & 0 & 0 & 0 \end{pmatrix} \tag{16}$$

This condition is strictly a symmetry condition, but is often used at inviscid walls in practice.

For subsonic inflow method n-INF2, the selection matrix extracts the outgoing characteristic equation at the inflow boundary, while three other conditions (total enthalpy, entropy, and tangential velocity) are prescribed. Here we wish to select the equation associated with the outgoing $u_n - c$ wave. To accomplish this, the Euler equations are first rotated to a coordinate system with components normal (n) and tangential (t) to the boundary,

$$R\left(\frac{\partial Q}{\partial \tau} + \frac{\partial F_x}{\partial x} + \frac{\partial F_y}{\partial y}\right) = \frac{\partial Q'}{\partial \tau} + \frac{\partial F_n}{\partial n} + \frac{\partial F_t}{\partial t} = 0. \tag{17}$$

Here, the definitions of the rotation matrix, rotated solution, and flux vectors are

$$R = \begin{pmatrix} 1 & 0 & 0 & 0 \\ 0 & n_x & n_y & 0 \\ 0 & -n_y & n_x & 0 \\ 0 & 0 & 0 & 1 \end{pmatrix}, \quad Q' = RQ = \begin{pmatrix} \rho \\ \rho u_n \\ \rho u_t \\ \rho e \end{pmatrix}, \quad F_n = \begin{pmatrix} \rho u_n \\ \rho u_n^2 + p \\ \rho u_n u_t \\ \rho u_n h \end{pmatrix}, \quad F_t = \begin{pmatrix} \rho u_t \\ \rho u_t u_n \\ \rho u_t^2 + p \\ \rho u_t h \end{pmatrix}. \tag{18}$$

Equation 17 is then multiplied by the modal matrix, M_n^{-1}, containing the right Eigenvectors of the normal flux Jacobian, $A_n = \partial F_n/\partial Q'$. Using the fact that $M_n^{-1} A_n M_n = \Lambda_n = \mathrm{diag}(u_n, u_n, u_n + c, u_n - c)$, leads to

$$\frac{\partial \hat{Q}'}{\partial \tau} + \Lambda_n \frac{\partial \hat{Q}'}{\partial n} + M_n^{-1} A_t M_n \frac{\partial \hat{Q}'}{\partial t} = 0, \tag{19}$$

where $\hat{Q}' = M_n^{-1} RQ$. It is clear from this form that the fourth equation represents the characteristic wave equation leaving the boundary. We wish to select this equation as part of the boundary specification. This

can be accomplished by defining the selection matrix as

$$A = \begin{pmatrix} 0 & 0 & 0 & 0 \\ 0 & 0 & 0 & 0 \\ 0 & 0 & 0 & 0 \\ 0 & 0 & 0 & 1 \end{pmatrix} M_n^{-1} R, \tag{20}$$

where

$$M_n^{-1} R = \begin{pmatrix} 1 - \frac{(\gamma-1)q^2}{2c^2} & (\gamma-1)\frac{u}{c^2} & (\gamma-1)\frac{v}{c^2} & -\frac{\gamma-1}{c^2} \\ u_t & n_y & -n_x & 0 \\ \frac{1}{2c^2}(\frac{\gamma-1}{2}q^2 - cu_n) & \frac{1}{2c^2}(n_x c - (\gamma-1)u) & \frac{1}{2c^2}(n_y c - (\gamma-1)v) & \frac{\gamma-1}{2c^2} \\ \frac{1}{2c^2}(\frac{\gamma-1}{2}q^2 + cu_n) & -\frac{1}{2c^2}(n_x c + (\gamma-1)u) & -\frac{1}{2c^2}(n_y c + (\gamma-1)v) & \frac{\gamma-1}{2c^2} \end{pmatrix} \tag{21}$$

The matrix $M_n^{-1}R$ is equivalent to $n_x M_x^{-1} + n_y M_y^{-1}$, where M_x^{-1} and M_y^{-1} are the modal matrices of the Cartesian flux Jacobians, $A_x = \partial F_x/\partial Q$ and $A_y = \partial F_y/\partial Q$, respectively. The n-INF2 condition is completed by specifying total enthalpy, entropy, and tangential velocity:

$$\Omega_D(Q) = \begin{pmatrix} h - h_{spec} \\ s - s_{spec} \\ u_t - u_{t,spec} \\ 0 \end{pmatrix}, \quad \Omega_N(Q) = 0, \quad \Omega_E(Q) = 0. \tag{22}$$

The outflow case n-OUT2 is based on a similar approach as n-INF2, but selects the remaining three characteristics at the outflow, while fixing the static pressure:

$$\Omega_D(Q) = \begin{pmatrix} 0 \\ 0 \\ 0 \\ p - p_{spec} \end{pmatrix}, \quad \Omega_N(Q) = 0, \quad \Omega_E(Q) = 0, \quad A = \begin{pmatrix} 1 & 0 & 0 & 0 \\ 0 & 1 & 0 & 0 \\ 0 & 0 & 1 & 0 \\ 0 & 0 & 0 & 0 \end{pmatrix} M_n^{-1} R \tag{23}$$

2.1.3 Weak Form Flux Implementation

A final method of boundary implementation suitable for node-centered schemes is through a modification of the flux. Traditionally, this has been used at an inviscid wall by setting the convective portion to zero and retaining only the pressure terms [2]:

$$F_n = \begin{pmatrix} 0 \\ pn_x \\ pn_y \\ 0 \end{pmatrix}. \tag{24}$$

Here, F_n is the directional flux at a boundary face with normal $\boldsymbol{n} = (n_x, n_y)^T$. We denote this method n-INV4 in Table 1.

It is interesting to note that this method does not explicitly involve a boundary residual, and thus cannot be verified using MMS and source terms as the other methods allow. Nonetheless, our results show that this method performs very well as shown through grid refinement studies using exact solutions. It is also interesting to note that this method does provide a water-tight formulation for node-centered schemes using inviscid walls.

2.2 Cell-Centered Boundaries

Unlike node-centered schemes, cell-centered schemes do not contain unknowns that lie directly on the boundary. Instead, ghost nodes are introduced, as shown in Figure 1(b). These ghost nodes do not lie within control volumes and do not contain flux balances from the governing equations. For this reason, it is difficult to apply any discretized equations of motion (e.g. mass, momentum, or energy) at boundary locations. It is at these ghost node locations that the boundary residual must be satisfied at steady-state. Because of the difficulty of obtaining discretized equations of motion at ghost nodes, we limit the boundary condition

choices to a combination of Dirichlet, Neumann, or extrapolation conditions:

$$R_b(Q) = \Omega(Q) = \Omega_D(Q) + \Omega_N(Q) + \Omega_E(Q). \tag{25}$$

These conditions may also be verified using MMS by adding a source term to the boundary residual:

$$R_b(Q) = \Omega(Q) - S_b(\boldsymbol{x}). \tag{26}$$

An important point is that for extrapolation conditions, the source term should be set to zero. This is because in the limit of grid refinement, the extrapolated value will equal the manufactured solution exactly.

We test six cell-centered boundary conditions that make use of the ghost node method. These are denoted c-INV1, c-INV3, c-INF1, c-INF2, c-OUT1, and c-OUT2 in Table 1. Method c-INV1 for an inviscid wall sets the normal velocity to zero, while extrapolating density, tangential velocity, and total energy:

$$\Omega_D(Q) = \begin{pmatrix} 0 \\ 0 \\ u_n \\ 0 \end{pmatrix}, \quad \Omega_N(Q) = 0, \quad \Omega_E(Q) = \begin{pmatrix} \rho - \rho_E \\ u_t - u_{tE} \\ 0 \\ \rho e - (\rho e)_E \end{pmatrix}. \tag{27}$$

Here, the subscript E refers to the state (linearly) extrapolated from the interior of the domain.

Method c-INV3 for an inviscid wall sets the normal velocity to zero, but uses Neumann conditions for density, tangential velocity, and total energy:

$$\Omega_D(Q) = \begin{pmatrix} 0 \\ 0 \\ u_n \\ 0 \end{pmatrix}, \quad \Omega_N(Q) = \begin{pmatrix} \partial\rho/\partial n \\ \partial u_t/\partial n \\ 0 \\ \partial(\rho e)/\partial n \end{pmatrix}, \quad \Omega_E(Q) = 0. \tag{28}$$

The Neumann conditions may be more appropriate for a symmetry condition, but this is often used for an inviscid wall in practice.

Method c-INF1 for subsonic inflow fixes the thermodynamic stagnation state and incoming tangential velocity, while extrapolating the velocity normal to the boundary:

$$\Omega_D(Q) = \begin{pmatrix} h - h_{spec} \\ s - s_{spec} \\ u_t - u_{t,spec} \\ 0 \end{pmatrix}, \quad \Omega_N(Q) = 0, \quad \Omega_E(Q) = \begin{pmatrix} 0 \\ 0 \\ 0 \\ u_n - u_{nE} \end{pmatrix}. \tag{29}$$

Method c-INF2 for subsonic inflow uses Riemann invariants normal to the boundary, entropy, and tangential velocity. The Riemann invariants have the usual definition for an ideal gas,

$$R^+ = u_n + \frac{2c}{\gamma - 1}, \quad R^- = u_n - \frac{2c}{\gamma - 1}, \tag{30}$$

where c is the speed of sound. The boundary condition then becomes,

$$\Omega_D(Q) = \begin{pmatrix} 0 \\ R^- - R^-_{spec} \\ u_t - u_{t,spec} \\ s - s_{spec} \end{pmatrix}, \quad \Omega_N(Q) = 0, \quad \Omega_E(Q) = \begin{pmatrix} R^+ - R^+_E \\ 0 \\ 0 \\ 0 \end{pmatrix} \tag{31}$$

The subsonic outflow condition c-OUT1 specifies the static pressure, and extrapolates density and velocity:

$$\Omega_D(Q) = \begin{pmatrix} 0 \\ 0 \\ 0 \\ p - p_{spec} \end{pmatrix}, \quad \Omega_N(Q) = 0, \quad \Omega_E(Q) = \begin{pmatrix} \rho - \rho_E \\ u - u_E \\ v - v_E \\ 0 \end{pmatrix}. \tag{32}$$

The subsonic outflow condition c-OUT2 is similar to c-INF2, but extrapolates tangential velocity and entropy to be consistent with the number of characteristics leaving the domain:

$$\Omega_D(Q) = \begin{pmatrix} 0 \\ R^- - R^-_{spec} \\ 0 \\ 0 \end{pmatrix}, \quad \Omega_N(Q) = 0, \quad \Omega_E(Q) = \begin{pmatrix} R^+ - R^+_E \\ 0 \\ u_t - u_{tE} \\ s - s_E \end{pmatrix}. \tag{33}$$

The final condition listed in Table 1 is c-INV2. This condition is similar to n-INV4, which weakly modifies the flux at the boundary to only contain the pressure terms, as in Equation 24. Thus only pressure needs to be extrapolated. As in n-INV4, it is not clear what the boundary residual is for this method. Thus, it is difficult to verify the method using MMS and source terms as the other methods allow.

3 Results

In this section we present results of the various boundary condition implementations in one and two dimensions for node- and cell-centered schemes. Four cases are considered: (1) quasi-1D nozzle flow, (2) 2D manufactured Euler solution in a square domain, (3) Ringleb Flow, and (4) subsonic flow over a NACA 0012 airfoil. For all cases, we perform grid refinement studies with the various boundary conditions listed in Table 1. At times, certain schemes fail to produce second-order results, in which cases explanations are given to account for these observations.

3.1 Quasi-1D Euler Equations

The quasi-1D Euler equations are a 1D formulation with added cross sectional area, $a(x)$, useful for nozzle flows. The quasi-1D Euler equations are defined as:

$$\frac{\partial Q}{\partial t} + \frac{\partial F}{\partial x} = S_p \tag{34}$$

$$Q = a \begin{pmatrix} \rho \\ \rho u \\ \rho e \end{pmatrix}, F = a \begin{pmatrix} \rho u \\ \rho u^2 + p \\ \rho u h \end{pmatrix}, S_p = \begin{pmatrix} 0 \\ \frac{\partial a}{\partial x} p \\ 0 \end{pmatrix} \tag{35}$$

In addition we assume ideal gases and constant specific heats. For the area, we use

$$a(x) = a_0 \left(1 + \frac{1}{2} cos(2\pi x)\right), \tag{36}$$

where $a_0 = 2/3$ to make the inlet and outlet area unity. In addition, the domain extents are $x \in [0, 1]$. A 2D view of the nozzle can be seen in Figure 2.

We solve the governing equations using a node-centered approach to test inflow and outflow conditions n-INF1, n-INF2, n-OUT1, and n-OUT2. Reduction of these methods from two dimensions to one dimension is straightforward. In order to verify the accuracy of the boundary methods, we consider the exact solution, which for fully subsonic flow, may be found simply from preserving constant entropy, enthalpy, and mass flux. For all tests, $M = 0.15$ was selected at the inflow to ensure subsonic flow at the throat.

While the quasi-1D Euler equations possess exact solutions, we also formulate a manufactured solution to test our MMS verification procedure of boundary conditions. The manufactured solution is chosen as

$$\begin{aligned} \rho^{MMS}(x) &= c_1 + c_{x1} sin(a_{x1} x) \\ u^{MMS}(x) &= c_2 + c_{x2} cos(a_{x2} x) \\ p^{MMS}(x) &= c_3 + c_{x3} sin(a_{x3} x) \end{aligned} \tag{37}$$

Figure 2: Converging-diverging nozzle used for the Quasi-1D Euler equations.

These constants are selected such that the manufactured solution remains physically meaningful (e.g. positive density). The period of the sinusoidal oscillation is set to approximately 20 times the length scale of the problem to ensure a smooth solution in the asymptotic range of convergence. Values for the constants are shown in table 2.

Constant	Value
c_1	1.0
c_{x1}	0.15
a_{x1}	0.075π
c_2	70.0
c_{x2}	7.0
a_{x2}	0.15π
c_3	1.0×10^{-5}
c_{x3}	2.0×10^{-4}
a_{x3}	0.1π

Table 2: A list of the MMS constants used in Equation 37 for the quasi-1D Euler solution verification.

With these manufactured solutions defined, it is necessary for us to determine the accompanying source terms, $S(x)$ and $S_b(x)$, in Equation 14. The interior source terms are computed in the usual manner by setting the source terms to the residual quantity remaining after the manufactured solution is substituted in the governing equations. The boundary source term is computed in a similar fashion, but considering only the boundary equations, such that

$$S_b = \Omega(Q^{MMS}), \tag{38}$$

where Q^{MMS} is the chosen manufactured solution. For example, the n-OUT2 condition, which specifies the exit pressure requires a boundary source term computed with

$$S_b = \Omega(Q^{MMS}) = \begin{pmatrix} 0 \\ 0 \\ p^{MMS} - p_{spec} \end{pmatrix} \tag{39}$$

With these definitions of S and S_b is then possible to solve Equation 12 to verify the interior scheme and boundary conditions simultaneously using MMS.

The results of the grid refinement study using the exact and manufactured solutions for the quasi-1D nozzle are shown in Figure 3. All methods produce second order accurate results. These results highlight two important points. First, the choice of boundary conditions that lead to consistent formulations does not appear to be unique. In this case the Lagrange multiplier method and the characteristic matrix selection method produce different equations. However, both equation sets lead to second-order accuracy. While the choice of equations is not unique, later we show examples of boundary conditions that are definitely wrong

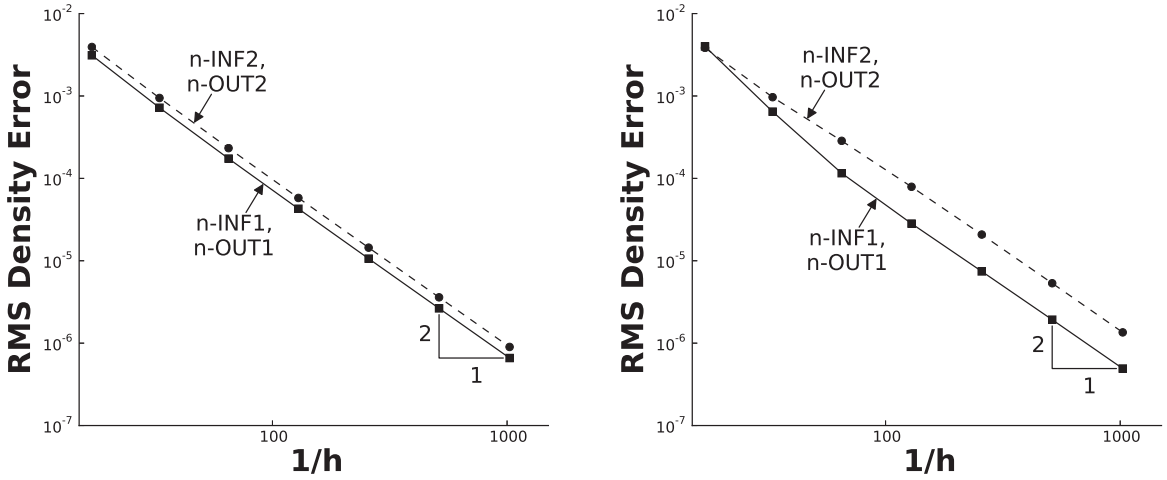

(a) Error obtained from exact solution

(b) Error obtained from manufactured solution

Figure 3: Grid refinement study for quasi-1D Euler equations using methods n-INF1, n-INF2, n-OUT1, and n-OUT2 with exact and manufactured solutions.

and degrade the accuracy.

A second important point is that the MMS procedure provides reliable information regarding the accuracy of the boundary formulation. In this case, an exact solution is available. However, in the vast majority of cases that use more complex equations and boundary conditions, exact solutions are not available. In these cases, the MMS procedure provides a straightforward way to measure the accuracy of boundary conditions. By determining the proper forms of $S(x)$ and $S_b(x)$, it is possible to use an arbitrary manufactured solution to verify boundary conditions along with the interior scheme. The next case highlights some important considerations when choosing forms for the manufactured solution.

3.2 Manufactured Solution in Square Domain

Here, we extend the ideas above to two-dimensional flows and further explore verification via manufactured solutions on a simple square domain. We consider the unit square domain shown in Figure 4. The domain is discretized with perturbed triangular cells, shown in Figure 4(a), to avoid any fortunate cancellation of solution error due to grid regularity. Velocity vectors for the chosen manufactured solution is shown in Figure 4(b). The manufactured solution follows a sinusoidal form similar to the solution used for the quasi-1D nozzle flow. An example for density is:

$$\rho(x, y) = c_1 + c_{x1} sin(a_{x1} x) + c_{y1} sin(a_{y1} y) + c_{xy1} cos(a_{xy1} xy). \tag{40}$$

Here the constants are chosen to be physically meaningful in some sense. The other flow variables (u, v, p) use similar forms. For the computation of source terms in multiple dimensions it is essentially necessary to use a symbolic math tool, such as the one contained in Matlab.

We systematically test the accuracy of various boundary conditions from Table 1 in isolation. To isolate a given boundary type, pure Dirichlet conditions were enforced on all the other boundaries of the domain except the one in question. The inviscid wall cases (INV) were applied on the top of the domain, inflow (INF) on the left side, and outflow (OUT) on the right side. With some of the methods (n-INV4 and c-INV2) it is not possible to apply the MMS procedure since it is unclear what the exact governing equations are for these weak forms.

Figure 5 shows the results of the tests performed for all the available MMS boundary types for node- and cell-centered methods. Figures 5(a) and 5(c) show the results for the isolated inviscid wall for both discretization schemes. The inflow and outflow results are combined into Figures 5(b) and 5(d) for node- and cell-centered methods respectively. The grid refinement study shows that Dirichlet, Neumann, extrapolation,

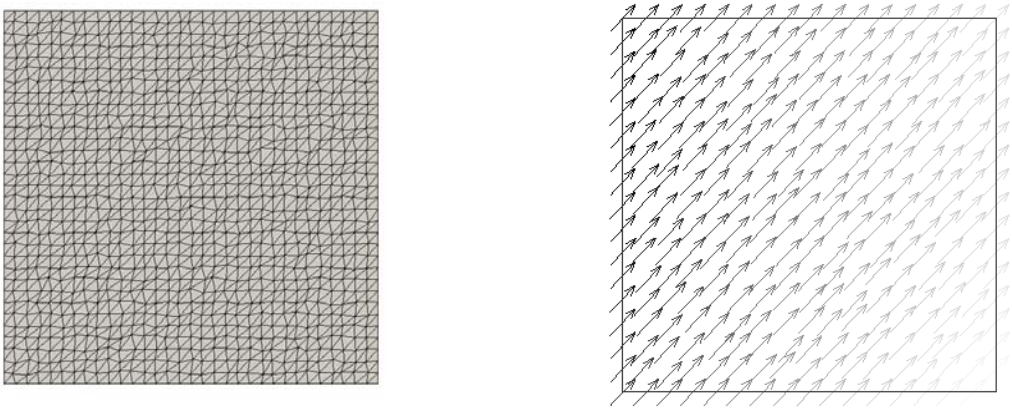

(a) 32×32 perturbed triangular mesh

(b) Manufactured solution velocity vectors.

Figure 4: Mesh and manufactured solution used for boundary condition verification.

and the equations of motion themselves are all reliable second-order accurate boundary conditions. The MMS procedures proves successful at verifying the proper implementation of the interior and boundary governing equations. A subtle but important point is that this procedure assumes the boundary normal vectors are exact at the nodes for the node-centered scheme. This assumption will be investigated further.

One important consideration when using MMS verification for boundary conditions is the characteristic directions of chosen manufactured solution. This is illustrated by considering inviscid wall conditions. Figure 4(b) illustrates that we have chosen the flow constants such that we obtain flow diagonally towards the upper-right of the domain. Because an inviscid wall specifies one piece of information ($u_n = 0$), this limits the location at which we can implement MMS verification for an inviscid wall to the top of the domain. This was our procedure for all the results obtained above. Placing the inviscid wall condition at the bottom of the square domain violates the wave propagation characteristics of the manufactured solution because it would require three specified pieces of information, not one. The effect of this phenomenon is shown in Figure 6, which shows the comparison of density error for an inviscid wall (c-INV3) at the top and bottom of the domain. It is noteworthy to mention that other inviscid wall boundary formulations (n-INV1-3) would not converge when enforced at the bottom of the domain due to stability issues. It is therefore critical that the manufactured solution and boundaries are chosen such that the characteristic direction is not violated for verification to be successful.

3.3 Ringleb Flow

In the previous section it was shown that all boundary condition methods tested are second order accurate using the method of manufactured solutions. We could not test methods n-INV4 and c-INV2 because we do not know the form of the underlying boundary residual, R_b. Here, we examine the same methods, including n-INV4 and c-INV2, using Ringleb flow [17], which is an exact solution of the Euler equations. The results of this test case highlight the importance of selecting physically correct conditions for a given problem. Just because a particular boundary condition is implemented in a mathematically consistent way (passes an MMS verification test for example), does not mean that it is the correct boundary condition for a given set of physics. Additionally, we highlight the difficulties of using derived quantities, such as entropy, as measures of solution error. Finally, this case also reveals the importance of computing boundary normals correctly for certain node-centered methods.

Ringleb flow describes inviscid compressible flow turning 180^o and involves subsonic, transonic, and supersonic regimes. Here, we focus on a subsonic portion of the flow. The exact solution is obtained via a

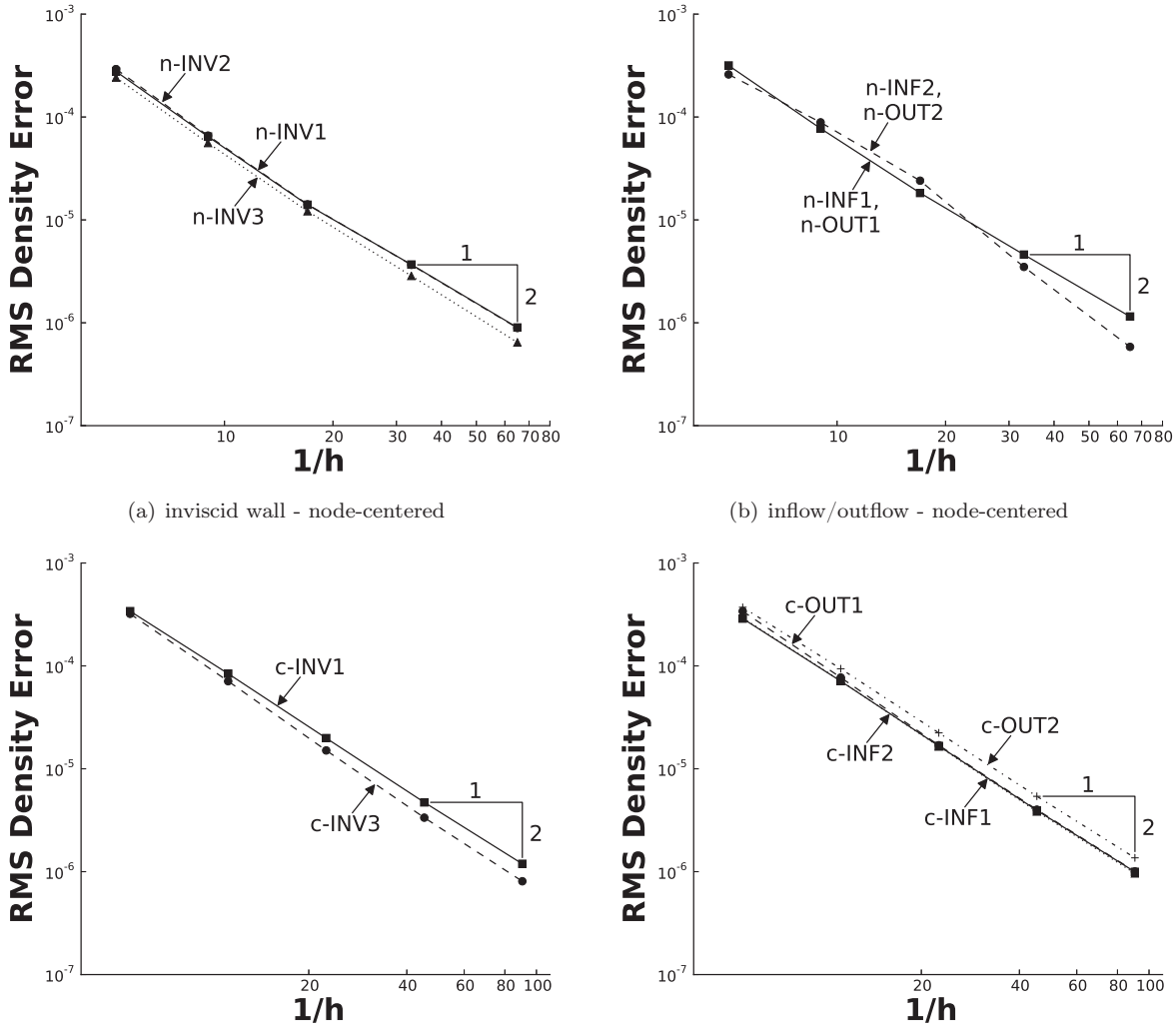

(a) inviscid wall - node-centered

(b) inflow/outflow - node-centered

(c) inviscid wall - cell-centered

(d) inflow/outflow - cell-centered

Figure 5: Grid refinement study for a variety of boundary formulations using MMS.

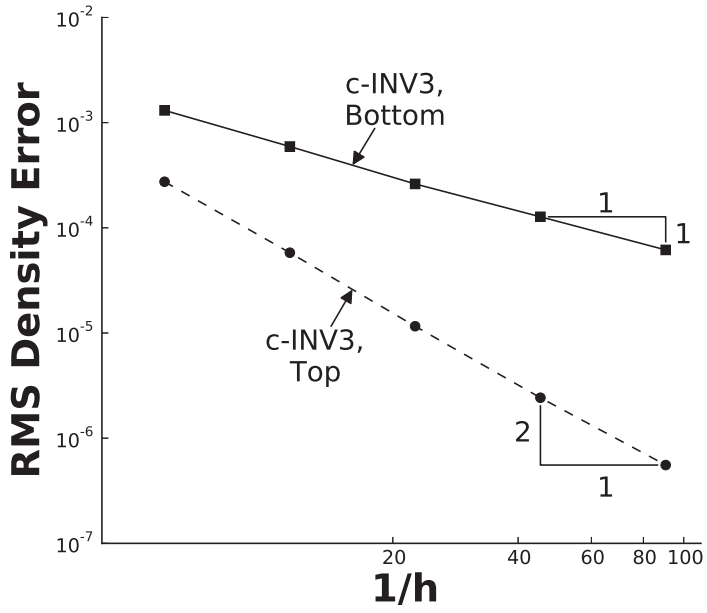

Figure 6: Example of the violation of characteristic directions for MMS solutions

hodograph method in the form of (x, y) coordinates parameterized by velocity magnitude, q, and streamline constant, k, which is the inverse of the stream function, $\psi = \frac{1}{q}\sin\theta$. Here, θ is the flow angle. The solution may be expressed as

$$x(q,k) = \frac{1}{2\rho}\left(\frac{1}{q^2} - \frac{2}{k^2}\right) + \frac{J}{2} \tag{41}$$

$$y(q,k) = \pm\frac{1}{kq\rho}\sqrt{1 - \frac{q^2}{k^2}}, \tag{42}$$

where

$$\begin{aligned} J &= \frac{1}{c} + \frac{1}{3c^3} + \frac{1}{5c^5} - \frac{1}{2}\log\left(\frac{1+c}{1-c}\right) \\ c &= \sqrt{1 - \frac{\gamma-1}{2}q^2} \\ \rho &= c^{\frac{2}{\gamma-1}}. \end{aligned}$$

Given a location (x, y), it is possible to solve for the corresponding (q, k) pair with a few Newton iterations. We dimensionalize the flow solution with desired stagnation quantities.

A series of increasingly refined meshes is used to verify the accuracy of boundary conditions. The mesh and exact solution for Ringleb flow are shown in Figure 7. The domain consists of two streamlines, which are treated as inviscid walls, as well as an inflow and outflow at the bottom and top portions of the domain, as shown in Figure 7(a). We test each boundary type in isolation by enforcing Dirichlet conditions on all boundaries but the one in question. The symmetric density contours of the exact solution are shown in Figure 7(b).

Figures 8-9 show the results for all boundary conditions listed in Table 1. Four important observations are made in reference to these figures. First, we observe in Figures 8(a) and 8(c) a substantial decrease in accuracy for the n-INV2, n-INV3 and c-INV3 cases. These three conditions, which were all verified as second-order accurate using MMS, now exhibit first-order accuracy when applied to Ringleb flow. At first this seems surprising, but may be explained by the fact that the MMS verification only addresses

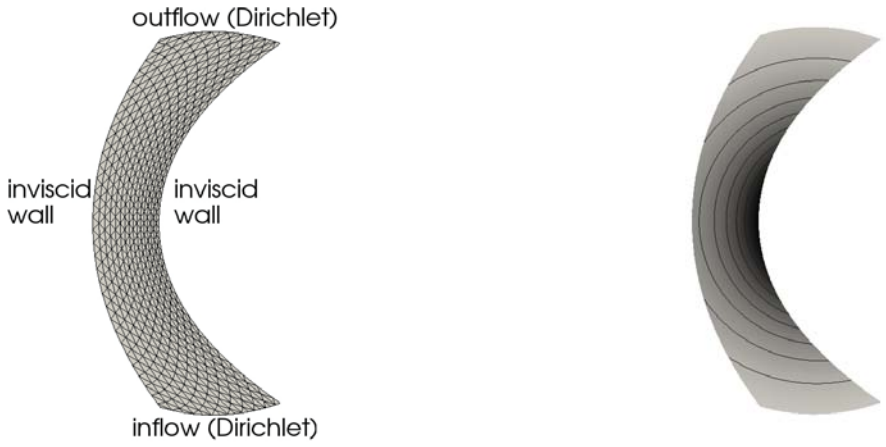

(a) 16 x 32 triangular mesh.

(b) Field plot of Ringleb flow density field.

Figure 7: Configuration for Ringleb flow test case.

the mathematical correctness of the discretization of the chosen conditions, not the appropriateness of the conditions themselves. In all three failed methods, Neumann terms are included in the inviscid boundary conditions. The Neumann conditions are rather arbitrary and do not correctly represent the physics for this case. In fact, they are in direct conflict with the governing Euler equations, which explains the reduced accuracy. This case illustrates the critical importance of selecting appropriate boundary conditions for a given set of physics.

A second observation is made by examining Figure 8(a), which shows the effect of approximating the boundary normal vector at nodal locations for method n-INV1. For Ringleb flow, the exact normal vectors may be deduced from the exact solution, which provides x and y locations along the inviscid wall streamline boundaries. We compute these exact normals and observe the effect on the accuracy compared to the approximate normal vectors computed as the average of the surrounding face normals at a node. We observe that using exact normals and approximate normals both result in second-order behavior. However, the level of error using exact normals is nearly half the error using approximate normals. For other cases with more complex geometry, the effects may be amplified. Methods to compute boundary normals consistently for complex geometry is an area of future work.

A third observation is that all inflow and outflow conditions tested show sharp second-order accuracy, as shown in Figures 8(b) and 8(d). All of these methods are physically meaningful and compatible with the current problem. Thus, the MMS results for these conditions are validated. Again, this demonstrates that the MMS verification procedure is sufficient if physically consistent boundary equations are used. This is important because it provides a method for the verification of more complex boundary conditions and interior schemes for which no exact solutions are known, such as averaged equations with turbulence models, multiphase flow models, or combustion.

Finally, it is interesting to consider the impact of the boundary discretizations on other quantities besides the conserved variables, such as entropy. Entropy is sometimes used as a measure of error for inviscid flow cases for uniform inflow [18, 19, 20]. Figure 9 shows the convergence of surface entropy for all inviscid wall conditions in Table 1. This figure shows that none of the methods are truly second order accurate considering the entropy. Recall that many of the methods were second order accurate considering the error in the conserved variables, as shown in Figures 8(a) and 8(c). This may be explained by the fact that isentropic flow is only attained if *all* the conservation laws are satisfied at all degrees of freedom. At the boundary locations, we do not solve the full set of conservations laws. Thus, entropy may not demonstrate the same convergence behavior as the mesh is refined. It may be possible to formulate boundary conditions which preserve specific flow features, such as isentropic flow. For example, entropy-based boundary conditions have been explored by Balakrishnan and Fernandez [4]. The next case also highlights potential difficulties with

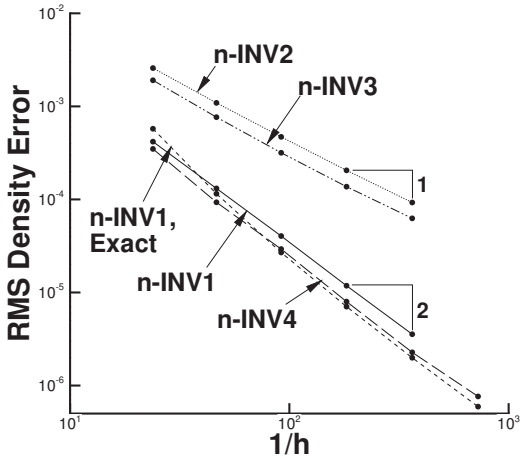

(a) Inviscid Wall - Node Centered

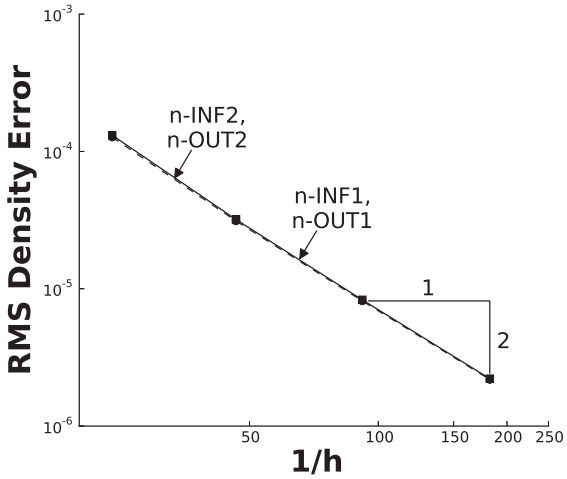

(b) Inflow/Outflow - Node Centered

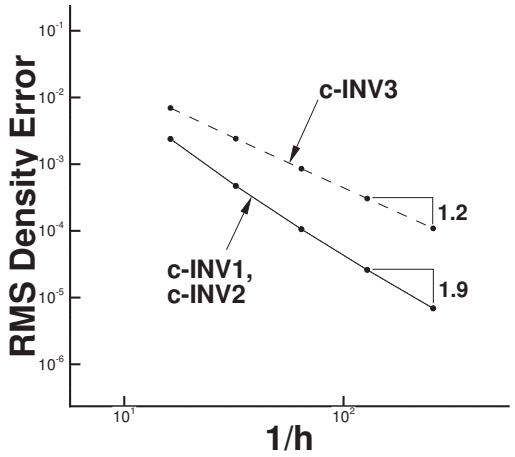

(c) Inviscid Wall - cell Centered

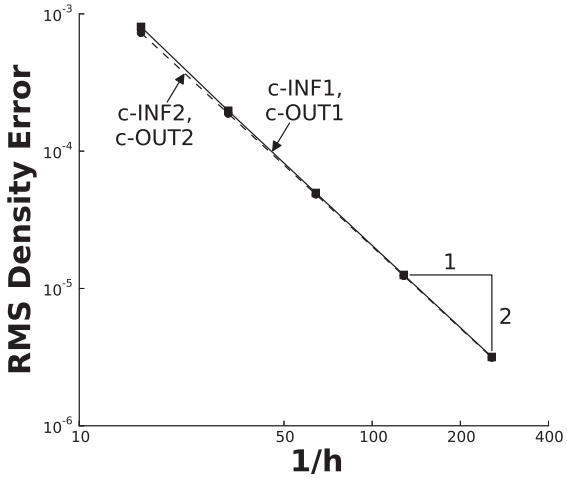

(d) Inflow/Outflow - Node Centered

Figure 8: Grid refinement study for various boundary formulations using Ringleb flow.

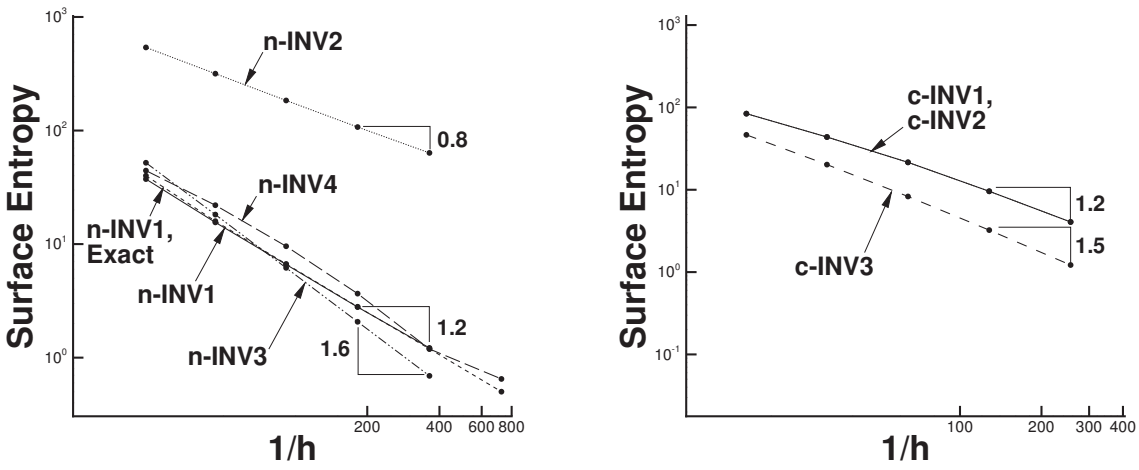

(a) Inviscid Wall - Node Centered

(b) Inviscid Wall - cell Centered

Figure 9: Grid refinement study for inviscid wall boundary formulations using Ringleb flow using entropy as a measure of error.

using entopy as a measure of error.

3.4 NACA 0012 Airfoil

The last case we present is inviscid flow over a NACA 0012 airfoil at $M = 0.5$ and $\alpha = 3.0^o$. We examine the effects of the various inviscid wall implementations in Table 1 on the entropy production at the airfoil surface as well as other qualitative aspects. We employ unstructured triangular grids with 40, 80, 160, and 320 surface points, respectively.

The results of the grid refinement test are shown in Figure 10 for both node- and cell-centered schemes. For the node-centered inviscid wall methods, similar trends can be seen in this case as are seen in the Ringleb flow case. Methods n-INV2 and n-INV3 clearly give first-order results. Initially, methods n-INV1 and nINV-4 appear to give second-order results. However, further refinement indicates first-order accuracy in the entropy, which is consistent with the Ringleb flow results. It is also clear from this case, that symmetry-type conditions are not suitable for inviscid walls. Qualitatively, errors in the Mach contours are apparent with the symmetry-type conditions as well. Figures 11(a)-11(b) show Mach contours for method n-INV1 and n-INV2, respectively. At the surface, method n-INV2 exhibits oddly-shaped Mach contours as a result of symmetry enforcement.

Like the node-centered schemes, the entropy produced from cell-centered schemes reduces between first- and second-order, as shown in Figure 10(b). However, this does not necessarily mean that the scheme is first-order in the conserved variables, as demonstrated bye the Ringleb flow case. Similar qualitative errors in the Mach contours can be seen for the node-centered symmetry conditions, as shown in Figures 11(a)-11(b). Similar Errors have been noted by Wang [19] and Barth [21]. The extrapolation condition in Figure 11(a) shows smooth Mach contours, while the symmetry condition in Figure 11(b) displays contour shape errors.

4 Conclusions

In this work, we present a general formulation for arbitrary boundary conditions for node- and cell-centered finite volume schemes. These conditions may include any combination of Dirichlet, Neumann, extrapolation, and, in the case of node-centered schemes, the equations of motion themselves. The ease with which we may apply the conservation equations of motion is one advantage of node-centered schemes over cell-centered schemes. This avoids the need for extrapolation or extra Neumann conditions which may conflict with the

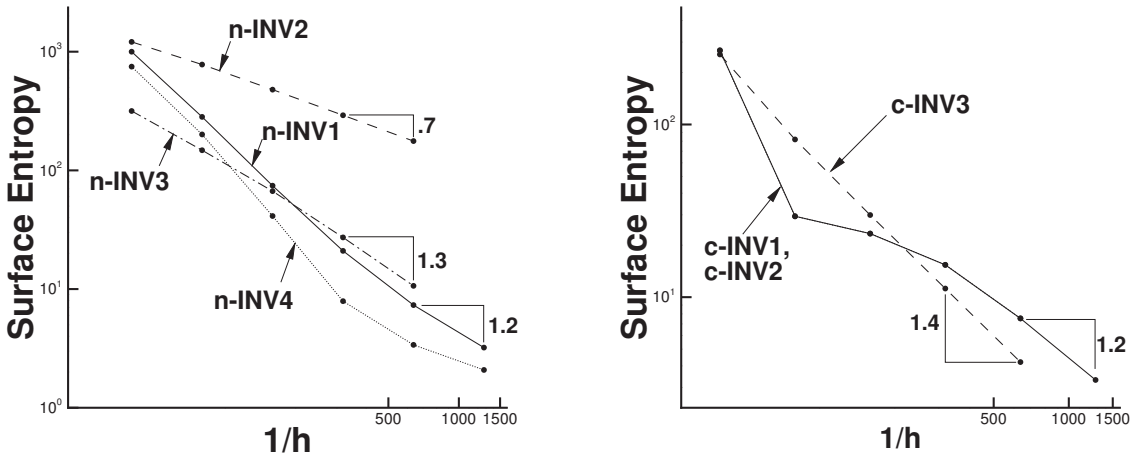

(a) Node-entered

(b) Cell-centered

Figure 10: Grid refinement study for various boundary formulations using flow around a NACA 0012 airfoil.

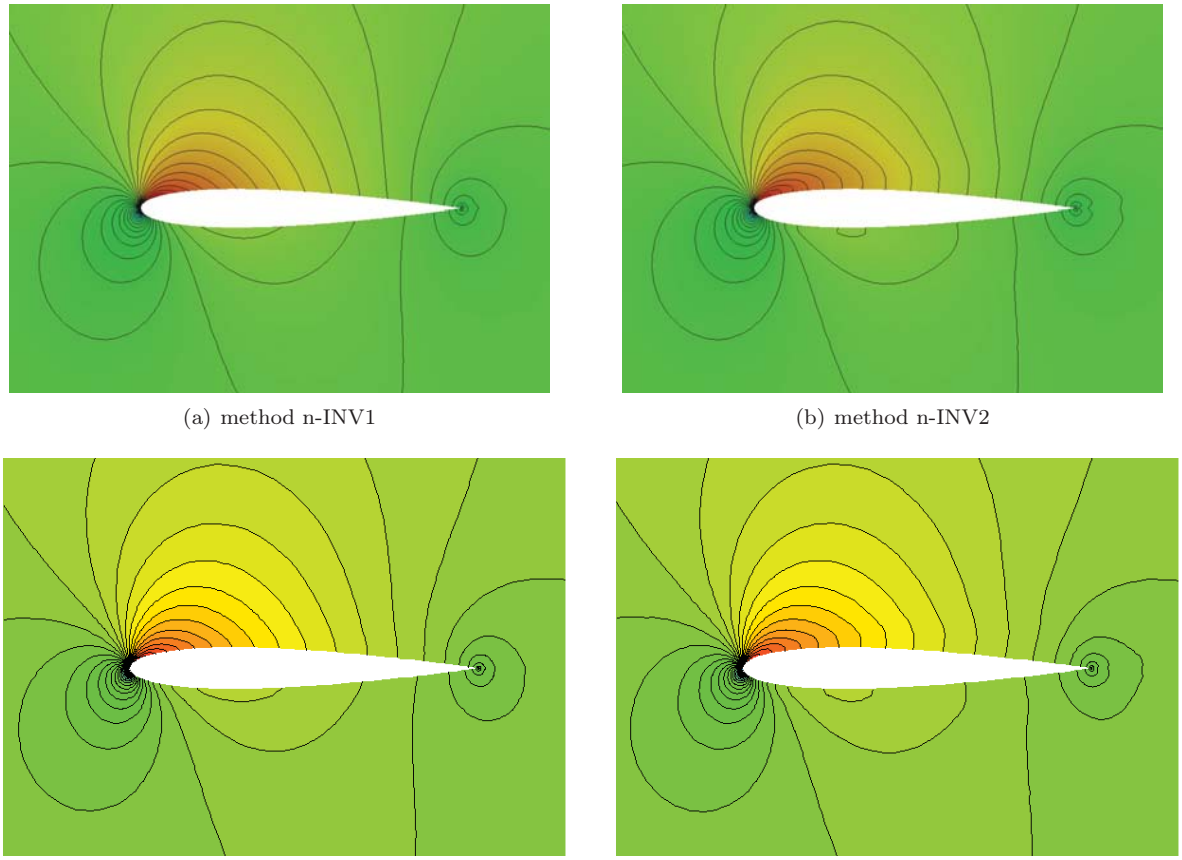

(a) method n-INV1

(b) method n-INV2

(c) method c-INV1

(d) method c-INV3

Figure 11: Mach contours for various inviscid wall treatments of a NACA 0012 inviscid airfoil at $M = 0.5$, $\alpha = 3.0^o$.

interior scheme or physical configuration of the problem.

Importantly, we extend the traditional use of the method of manufactured solutions to include boundary conditions. By defining a boundary residual equation to accompany the interior residual equation, MMS can be used in both node- and cell-centered contexts to verify the combined interior-boundary scheme. In this manner, a single manufactured solution can be used to verify any number of boundary conditions conveniently. Computation of boundary source terms is straightforward, generally requiring much less algebraic manipulation than interior source terms.

A number of test cases, including quasi-1D flow and fully 2D flow demonstrate the use of the MMS procedure. It is found that the manufactured solution must be chosen such that characteristic directions are respected during the boundary condition verification procedure. While the manufactured solution is arbitrary, boundary locations should be chosen to roughly coincide with the physics of the manufactured solution. If this practice is violated, erroneous results will be obtained or non-convergence will result.

While the correct choice of boundary conditions for a given problem is often not unique, a key finding from studies involving Ringleb flow and inviscid airfoils is that certain boundary conditions may conflict with the interior scheme or the problem configuration. An example is the use of Neumann symmetry conditions for inviscid walls. Even though the symmetry condition is verifiably second-order accurate using the MMS procedure, it fails to produce the proper results when applied in an inappropriate physical context. Thus, the MMS procedure is only valid when used with physical insight to apply boundary conditions in the correct way. If used correctly, the MMS procedure provides a method for the verification of complex boundary conditions and interior schemes for which no exact solutions are known. In addition, we find it is best to use the conserved variables directly to measure the solution error, as opposed to derived quantities, such as entropy. Entropy appears to converge as second-order only when all conservation laws are satisfied, which is not the case for the boundary methods investigated in this paper. It may be possible to formulate special entropy preserving boundary conditions, which preserve isentropic flow.

Future work will focus on modifications of the node-centered approach to allow for a water-tight flux formulation. One possible approach is to introduce ghost nodes into the node-centered formulation in a manner similar to the cell-centered formulation. Another important area of investigation includes consistent methods for boundary normal computation. A possible strategy includes locally reconstructing the surface description from surrounding geometry information using a least squares procedure. Derivatives of the reconstructed surface may then be used to estimate normal vectors.

5 Acknowledgments

Research for this work was supported by the Army Research Office (ARO), under the supervision of Dr. Frederick Ferguson. The authors would like to thank Dr. Ferguson for his continuing support of this research. Material presented in this paper is a product of the CREATE-AV Element of the Computational Research and Engineering for Acquisition Tools and Environments (CREATE) Program sponsored by the U.S. Department of Defense HPC Modernization Program Office. Dr. Robert Meakin is the program manager for CREATE-AV.

References

[1] A. Rizzi. Numerical implementation of solid body boundary conditions for the euler equations. *ZAMM*, S8:301–304, 1978.

[2] A. Jameson, T. Baker, and N. Weatherill. Calculation of inviscid transonic flow over a complete aircraft. *AIAA paper* 83-0103, AIAA 24th Aerospace Sciences Meeting, Reno, NV, January 1986.

[3] A. Dadone and B. Grossman. Surface boundary conditions for the numerical solution of the euler equations. *AIAA Journal*, 32:285–293, 1994.

[4] N. Balakrishnan and G. Fernandez. Wall boundary conditions for inviscid compressible flows on unstructured meshes. *Int. J. Numer. Meth. Fluids*, 28:1481–1501, 1998.

[5] A. Choudhary, C. Roy, E. Luke, and S. Veluri. Issues in verifying boundary conditions for 3d unstructured CFD codes. *AIAA paper* 2011-3868, AIAA 20th Computatonal Fluid Dynamics Conference, Honolulu, June 2011.

[6] A. Katz and V. Sankaran. Mesh quality effects on the accuracy of euler and navier-stokes solutions on unstructured meshes. Technical report, 6th International Conference on Computational Fluid Dynamics, St. Petersburg, Russia, July 2010.

[7] B. Diskin and J. Thomas. Accuracy analysis for mixed-element finite-volume discretization schemes. *NIA Report* 2007-08, National Institute of Aerospace, 2007.

[8] C. Roy. Review of code and solution verification procedures for computational simulation. *Journal of Computational Physics*, 205:131–156, 2005.

[9] E. Luke, S. Hebert, and D. Thompson. Theoretical and practical evaluation of solver-specific mesh quality. *AIAA paper* 2008-0934, AIAA 46th Aerospace Sciences Meeting, Reno, NV, January 2008.

[10] M. Giles. Accuracy of node-based solutions on irregular meshes. *Lecture Notes in Physics*, 323:273–277, 1989.

[11] Steven R. Allmaras. Lagrange Multiplier Implementation of Dirichlet Boundary Conditions in Compressible Navier-Stokes Finite Element Methods. *AIAA Computation Fluid Dynamics Conference*. AIAA 2005-4714.

[12] I. Babuska. Error-bounds for the finite element method. *Numer. Math.*, 16:322–333, 1971.

[13] A. Katz and V. Sankaran. Mesh quality effects on the accuracy of Euler and Navier-Stokes solutions on unstructured meshes. *Journal of Computational Physics*, 230(20):7670–7686, 2011.

[14] P. Tota and Z. J. Wang. Meshfree Euler solver using local radial basis functions for inviscid compressible flows. *AIAA paper* 2007-4581, AIAA 18th Computational Fluid Dynamics Conference, 2007.

[15] D. Kirshman and F. Liu. Gridless boundary condition treatment for a non-body-conforming mesh. *AIAA paper* 2002-3285, AIAA 32nd Fluid Dynamics Conference, St. Louis, MO, June 2002.

[16] E. Koh and H. Tsai. Euler solution using Cartesian grid with least squares technique. *AIAA paper* 2003-1120, AIAA 41st Aerospace Sciences Meeting, Reno, NV, January 2003.

[17] A. H. Shapiro. *The Dynamics and Thermodynamics of Compressible Fluid Flow*, volume 2. The Ronald Press Company, 1954.

[18] H. Luo, H. Xiao, R. Nourgaliev, and C. Cai. A comparative study of different reconstruction schemes for a reconstructed discontinuous Galerkin method on arbitrary grids. *AIAA paper* 2011-3839, AIAA 20th Computational Fluid Dynamics Conference, Honolulu, HI, June 2011.

[19] Z. J. Wang and Y. Sun. Curvature-based wall boundary condition for the Euler equations on unstructred grids. *AIAA paper* 2002-0966, AIAA 40th Aerospace Sciences Meeting, Reno, NV, January 2002.

[20] J. Andren, H. Gao, M. Yano, D. Darmofal, C. Ollivier-Gooch, and Z. Wang. A comparison of higher-order methods on a set of canonical aerodynamics applications. *AIAA paper* 2011-3230, AIAA 20th Computational Fluid Dynamics Conference, Honolulu, June 2011.

[21] T. J. Barth. Aspects of unstructured grids and finite-volume solvers for the Euler and Navier-Stokes equations. Technical report, von Karman Institute for Fluid Dynamics, Moffett Field, CA, March 1994.